Behaviour of motion of infinitesimal variable mass oblate body in the generalized perturbed circular restricted three-body problem

Abdullah A. Ansari*
International Center for Advanced Interdisciplinary Research (ICAIR)
Sangam Vihar, New Delhi
India
icairndin@gmail.com

Laxmi Narain
Department of Mathematics
Acharya Narendra Dev College
University of Delhi
Delhi
India
laxminarain@andc.du.ac.in

Sada Nand Prasad
Department of Mathematics
Acharya Narendra Dev College
University of Delhi
Delhi
India
sadanandprasad@andc.du.ac.in

Mehtab Alam
International Center for Advanced Interdisciplinary Research (ICAIR)
Sangam Vihar, New Delhi
India
mehtab_alam@live.com

Abstract. The main goal of the present study is to reveal the behaviour of motion of the infinitesimal body in case of circular restricted three-body problem where all the participating bodies have oblate shapes and both primaries have the effect of solar radiation pressure. The third infinitesimal body is varying its mass according to Jeans law. We also consider that the system is affected by the small perturbations in Coriolis and centrifugal forces. We evaluate the equations of motion of the infinitesimal oblate body under the generalized sense in the perturbed circular restricted three-body problem by using the Meshcherskii-space time transformations to preserve the dimensions of the position as well as time, and then determine the Jacobi-integral. Further we numerically illustrated the equilibrium points, Poincaré surfaces of section, regions of possible and forbidden motion and then basins of the attracting domain by supposing the effects of all the parameters used. Further more, we examine the stability of these

*. Corresponding author

equilibrium points with the help of Meshcherskii space-time inverse transformations and found them unstable.

Keywords: infinitesimal oblate body, variable mass, regions of forbidden motion, stability of equilibrium points.

1. Introduction

Plagiarism is a serious issue at the time of writing a research paper. We should directly focus towards our problem. Our research field is a part of Mechanics i.e. Celestial mechanics which also lies in the Applied Mathematics and theoretical Physics. Here, we have focused on the motion of the small particle (especially Satellite in comparison to the Earth) under the gravitational attraction of the other two celestial bodies i.e restricted three-body problem. Restricted means the two bigger primary bodies are influencing the third infinitesimal body with their forces but the third body will not affect the motion of the primaries. We also consider that both the primaries have solar radiation pressure as well as oblateness effect while the third infinitesimal body is taken as oblate in shape and varies its mass according to Jeans law. The system is perturbed by the Coriolis and centrifugal forces. The two primaries are moving in circular orbits around their common center of mass which is taken as origin. All these effects and perturbations are studied by many researchers separately as follows:

[25] numerically investigated the effect of oblateness of the more massive primary on the location of five equilibrium points in the circular restricted 3-body problem. They noticed that the patterns of angular frequencies have interesting differences. [17] investigated the effects of perturbations in the frame of restricted three-body problem and compared there work with the previous works. They found that these perturbations have significant impact on the stability of equilibrium points. [26, 27] investigated the effects of radiation pressure, oblateness, variable mass and asteroid belts in the framework of the circular restricted three-body problem by finding Lagrangian function with the help of kinetic energy and potential energy. [1] studied the effects of radiation pressure, oblateness as well as Coriolis and centrifugal forces on the stability of equilibrium points in the frame of circular restricted three-body problem. They observed that the Coriolis force has stabilizing tendency while other forces have destabilizing tendency. They also found that collinear equilibrium points are always unstable while non-collinear points are week in stability due to these external factors.

[21] investigated the effect of variable mass in the frame of circular restricted three-body problem by considering that sum of the masses of all bodies are always constant. They obtained the zero-velocity surfaces using Jacobi-quasi-integral. They also presented an example for their model as binary stars system with conservation of mass transfer. [18] revealed the existence, position and stability of the collinear equilibrium points in the frame of generalized Hill's problem by hypothesizing primary as radiating and secondary as oblate. They

also plotted the basins of attraction by using fast and simple Newton-Raphson iterative method for several cases of parameters. [23] investigated the effect of oblateness on the periodic orbits as well as on the regions of quasi-periodic motion around both the primaries in the circular restricted three-body problem by using the numerical technique of Poincaré surfaces of section. They found some variations in the stability of orbits due to oblateness. [29] studied the motion of infinitesimal variable mass in the circular restricted three-body problem by taking on account to one of the primaries having photo-gravitational effect using Jeans law [19] and Meshcharskii space-time transformations [22].

[20] analysed the motion of infinitesimal body in the frame of restricted four-body problem with solar wind drag and radiation pressure. They numerically studied the equilibrium points, zero-velocity curves, Poincaré surfaces of sections and Lyapunove Characteristic exponents (LCEs). [4, 2, 5, 6] studied the effect of oblateness, radiation pressure of the primaries as well as the effect of variable mass of the infinitesimal body in the frame of restricted problem. [24] explored the motion of the infinitesimal body around one of the triangular equilibrium points (L_4) in the circular restricted three-body problem by choosing one of the primary as Heterogeneous triaxial body. [8, 7, 9, 10, 11, 12, 13, 14, 16] investigated the effects of the perturbations and variable mass in the frame of restricted three-body problem. They also studied the effects of these perturbations on the locations of equilibrium points, Poincaré surfaces of section, regions of possible and forbidden motion, basins of attraction and examined the stability of these equilibrium points where most of the cases they found that these points are unstable. [30] investigated the basins of convergence of attracting points by considering the modified gravitational potential using well-known Newton-Raphson iterative method in the frame of restricted three-body problem. They also computed the degree of fractality using the basin entropy.

This work is organised in various sections and subsections which are as follows: The overview of literature is given in section 1. The determination of equations of motion and Jacobi-integral are given in section 2 while section 3 represent the numerical works with subsections 3.1, 3.2, 3.3 and 3.4. The stability of equilibrium points are numerically studied in section 4. Finally the conclusion of the work is presented in section 5.

2. Determination of equations of motion

Let there be three masses m_i and m where two masses (m_i) are primaries of oblate shapes with oblateness factors σ_i and radiation pressures with radiation factors q_i, (i = 1, 2) respectively while the third body has also oblate shape with oblateness factor σ and varies its mass according to Jeans law. We also considered that the motion is perturbed by the coriolis and centrifugal forces with factors ϕ and ψ respectively. In the synodic coordinate system xyz, the line joining both the primaries, is taken as x-axis while the line perpendicular to this line is considered as y-axis. The two primary bodies are moving in circular orbits

around their common center of mass which is taken as origin. The mean motion n of the system is taken about $z-axis$ which is perpendicular to the plane of motion of the primaries. The gravitational forces of primaries are influencing to the third infinitesimal variable mass oblate body while these two bodies are not influenced by the third body. To fix the variables as non-dimensional, assume that the total mass of the primaries is unity, the separation distance between the primaries (R) is unity and the time of unit is so chosen as the gravitational constant is also unity. i.e. $m_1+m_2=1$, $R=1$ and $G=1$. Let $\mu=\frac{m_2}{m_1+m_2}$ and $m_1=1-\mu$. The coordinates of the primaries(m_i) and the infinitesimal body (m) are given by $(-\mu,0,0)$, $(1-\mu,0,0)$ and (x,y,z) respectively. Following the procedure given by [3] and [15], we can illustrate the equations of motion of the infinitesimal variable mass oblate body with non-dimensional variables where the variation of mass of this body originates from one point and have zero momenta as:

$$
\begin{aligned}
V_x &= \frac{\dot{m}}{m}(\dot{x}-n\phi y)+(\ddot{x}-2n\phi\dot{y}),\\
V_y &= \frac{\dot{m}}{m}(\dot{y}+n\phi x)+(\ddot{y}+2n\phi\dot{x}),\\
V_z &= \frac{\dot{m}}{m}\dot{z}+\ddot{z},
\end{aligned}
\tag{1}
$$

where

$$
V=\frac{n^2\psi}{2}(x^2+y^2)+(1-\mu)\left(\frac{q_1}{r_1}+\frac{(q_1\sigma_1+\sigma)}{2r_1^3}\right)+\mu\left(\frac{q_2}{r_2}+\frac{(q_2\sigma_2+\sigma)}{2r_2^3}\right), \tag{2}
$$

with

$$
\begin{gathered}
r_1^2=(x+\mu)^2+y^2+z^2,\\
r_2^2=(x-1+\mu)^2+y^2+z^2,\\
n^2=1+\frac{3}{2}(\sigma_1+\sigma_2),\\
\phi=1+\epsilon_1,\\
\psi=1+\epsilon_2,\\
\epsilon_1,\epsilon_2\ll 1.
\end{gathered}
$$

Due to variation of mass, we should preserve the dimension of the space and time therefore we will use Jean's law [19] and Meshcherskii space time transformations [22] as,

$$
\begin{aligned}
&m=m_0e^{-\alpha_1 t}, dt=d\tau\\
&x=\alpha_2^{-1/2}\xi, \dot{x}=\alpha_2^{-1/2}\left(\dot{\xi}+\frac{\alpha_1}{2}\xi\right), \ddot{x}=\alpha_2^{-1/2}\left(\ddot{\xi}+\alpha_1\dot{\xi}+\frac{\alpha_1^2}{4}\xi\right)\\
&y=\alpha_2^{-1/2}\eta, \dot{y}=\alpha_2^{-1/2}\left(\dot{\eta}+\frac{\alpha_1}{2}\eta\right), \ddot{y}=\alpha_2^{-1/2}\left(\ddot{\eta}+\alpha_1\dot{\eta}+\frac{\alpha_1^2}{4}\eta\right)\\
&z=\alpha_2^{-1/2}\zeta, \dot{z}=\alpha_2^{-1/2}\left(\dot{\zeta}+\frac{\alpha_1}{2}\zeta\right), \ddot{z}=\alpha_2^{-1/2}\left(\ddot{\zeta}+\alpha_1\dot{\zeta}+\frac{\alpha_1^2}{4}\zeta\right),
\end{aligned}
\tag{3}
$$

where α_1 is constant coefficient, $\alpha_2 = \dfrac{m}{m_0}$ and m_0 is the mass of infinitesimal oblate body at time $t = 0$.

After using Eq.(3) in Eq. (1), we get

$$\begin{aligned} \frac{\partial \Omega}{\partial \xi} &= \ddot{\xi} - 2n\phi\dot{\eta}, \\ \frac{\partial \Omega}{\partial \eta} &= \ddot{\eta} + 2n\phi\dot{\xi}, \\ \frac{\partial \Omega}{\partial \zeta} &= \ddot{\zeta}, \end{aligned} \tag{4}$$

where

$$\begin{aligned} \Omega = &\frac{\alpha_1^2}{8}(\xi^2+\eta^2+\zeta^2) + \frac{n^2\psi}{2}(\xi^2+\eta^2) \\ &+ \alpha_2^{3/2}\left[(1-\mu)\{\frac{q_1}{\rho_1} + \frac{(q_1\sigma_1+\sigma)\alpha_2}{2\rho_3^3}\} + \mu\{\frac{q_2}{\rho_2} + \frac{(q_2\sigma_2+\sigma)\alpha_2}{2\rho_2^3}\}\right], \end{aligned} \tag{5}$$

with

$$\begin{aligned} \rho_1^2 &= (\xi + \mu\sqrt{\alpha_2})^2 + \eta^2 + \zeta^2, \\ \rho_2^2 &= (\xi - \sqrt{\alpha_2}(1-\mu))^2 + \eta^2 + \zeta^2. \end{aligned} \tag{6}$$

The equations of motion (4) admits as

$$\dot{\xi}^2 + \dot{\eta}^2 + \dot{\zeta}^2 = 2\Omega - C - 2\int_{t_0}^{t} \frac{\partial \Omega}{\partial t} dt, \tag{7}$$

where left hand side of Eq. (7) represents the velocity of the infinitesimal oblate body and C is the Jacobian constant for the system.

3. Numerical performances

3.1 Location of equilibrium points

We can find the locations of equilibrium points after putting all the derivatives to zero and solving the obtained equations of the system (4), i.e. $\Omega_\xi = 0$, $\Omega_\eta = 0$ and $\Omega_\zeta = 0$, and hence

$$\begin{aligned} &\xi(n^2\psi + \frac{\alpha_1^2}{4}) - \alpha_2^{3/2}\left(\frac{q_1(1-\mu)(\xi+\sqrt{\alpha_2}\mu)}{\rho_1^3} + \frac{3(\sigma+\sigma_1 q_1)\alpha_2(1-\mu)(\xi+\sqrt{\alpha_2}\mu)}{2\rho_1^5}\right) \\ &- \alpha_2^{3/2}\left(\frac{q_2\mu(\xi+\sqrt{\alpha_2}(-1+\mu))}{\rho_2^3} + \frac{3(\sigma+\sigma_2 q_2)\alpha_2\mu(\xi+\sqrt{\alpha_2}(-1+\mu))}{2\rho_2^5}\right) = 0, \end{aligned} \tag{8}$$

$$\eta(n^2\psi + \frac{\alpha_1^2}{4}) - \eta\alpha_2^{3/2}\left(\frac{q_1(1-\mu)}{\rho_1^3} + \frac{3(\sigma+\sigma_1 q_1)\alpha_2(1-\mu)}{2\rho_1^5}\right)$$
$$-\eta\alpha_2^{3/2}\left(\frac{q_2\mu}{\rho_2^3} + \frac{3(\sigma+\sigma_2 q_2)\alpha_2\mu}{2\rho_2^5}\right) = 0, \tag{9}$$

$$\zeta\frac{\alpha_1^2}{4} - \zeta\alpha_2^{3/2}\left(\frac{q_1(1-\mu)}{\rho_1^3} + \frac{3(\sigma+\sigma_1 q_1)\alpha_2(1-\mu)}{2\rho_1^5}\right)$$
$$-\zeta\alpha_2^{3/2}\left(\frac{q_2\mu}{\rho_2^3} + \frac{3(\sigma+\sigma_2 q_2)\alpha_2\mu}{2\rho_2^5}\right) = 0. \tag{10}$$

After numerically solving Eqs. (8), (9) and (10) for the variations of the parameters used with the help of well known software, Mathematica, we perform these graphs in Figures 1,2,3 and 4. We have illustrated these points in five cases as:

1. The Classical case:
   $(\sigma = 0, \sigma_1 = 0, \sigma_2 = 0,\ q_1 = 1, q_2 = 1,\ \epsilon_1 = 0, \epsilon_2 = 0,\ \alpha_1 = 0, \alpha_2 = 1)$

2. Taken the effect of oblateness of all three participating bodies:
   $(\sigma = 0.001, \sigma_1 = 0.003, \sigma_2 = 0.005,\ q_1 = 1, q_2 = 1,\ \epsilon_1 = 0, \epsilon_2 = 0,$
   $\alpha_1 = 0, \alpha_2 = 1)$

3. Taken the effect of oblateness and radiation pressure:
   $(\sigma = 0.001, \sigma_1 = 0.003, \sigma_2 = 0.005,\ q_1 = 0.85, q_2 = 0.95,\ \epsilon_1 = 0, \epsilon_2 = 0,$
   $\alpha_1 = 0, \alpha_2 = 1)$

4. Taken the effect of oblateness, radiation pressure, Coriolis and centrifugal forces:
   $(\sigma = 0.001, \sigma_1 = 0.003, \sigma_2 = 0.005,\ q_1 = 0.85, q_2 = 0.95,\ \epsilon_1 = 0.2, \epsilon_2 = 0.2,$
   $\alpha_1 = 0, \alpha_2 = 1)$

5. Taken the effect of all perturbations given in case 4 including the variation of mass parameters:
   $(\sigma = 0.001, \sigma_1 = 0.003, \sigma_2 = 0.005,\ q_1 = 0.85, q_2 = 0.95,\ \epsilon_1 = 0.2, \epsilon_2 = 0.2,$
   $\alpha_1 = 0.2, \alpha_2 \neq 1.)$

Figure (1) represents the variation of the cases from case 1 to case 5 in $\xi - \eta$-plane. Here the points due to the cases 1, 2, 3, 4 and 5 are denoted by black, green, magenta, orange and blue colors respectively. We introduced the cases one by one, further we observed from Figure (1(a)) that the system has five equilibrium points ($L_{1,2,3,4,5}$) out of which three ($L_{1,2,3}$) are collinear and two ($L_{4,5}$) are non-collinear (also known as triangular points), all these equilibrium points are moving towards origin. This effect can be easily seen in Figure 1(b) which is representing the zoomed part of the Figure 1(a) near L_4. Figure 2 presents the equilibrium points due to these five cases in $\xi - \zeta$-plane. From this

Figure we observed that due to first four cases there are only three collinear equilibrium points given in Figure 2(a) and found that due to these cases three equilibrium points ($L_{1,2,3}$) are moving towards origin while due to case 5 we receive two more equilibrium points ($L_{4,5}$) including the collinear equilibrium points ($L_{1,2,3}$) (Figure 2(b)).

In Figure 3, we perform the case 5 where we have seen the effect of variation of mass parameter α_1 (0.2 (Black), 0.4 (Green), 0.6 (Magenta)) in $\xi - \eta$-plane (Figure 3(a)) and in $\xi - \zeta$-plane (Figure 3(b)). The Figure 3(a) shows only slight variation in equilibrium points $L_{3,4,5}$ while there are no effect on the equilibrium points $L_{1,2}$ due to increase in the value of α_1. The Figure 3(b) shows as the value of α_1 increases, the three equilibrium points ($L_{1,2,3}$) remain unchanged while two equilibrium points $L_{4,5}$ are moving towards the origin. Figure 4 reveals the case 5 where we have seen the effect of variation of mass parameter α_2 (0.4 (black), 0.8 (green), 1.4 (magenta)) in $\xi - \eta$-plane (Figure 4(a)) and in $\xi - \zeta$-plane (Figure 4(b)). These two Figures 4(a) and 4(b) shows that as the value of α_2 increases, all five equilibrium points ($L_{1,2,3,4,5}$) move away from the origin. We also noticed that there is no effect of Coriolis force on the location of equilibrium points.

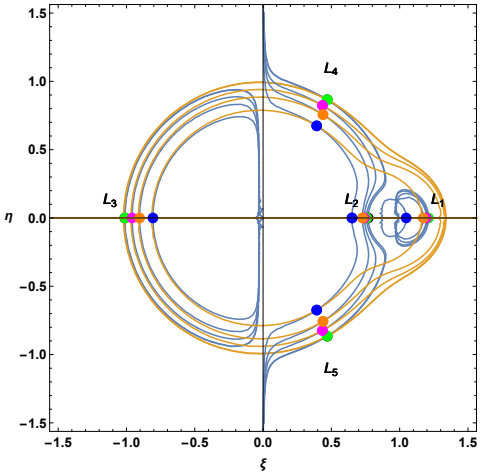

(a) Different color points show the variation of cases 1 (black), 2 (green), 3 (magenta), 4 (orange) and 5 (blue)

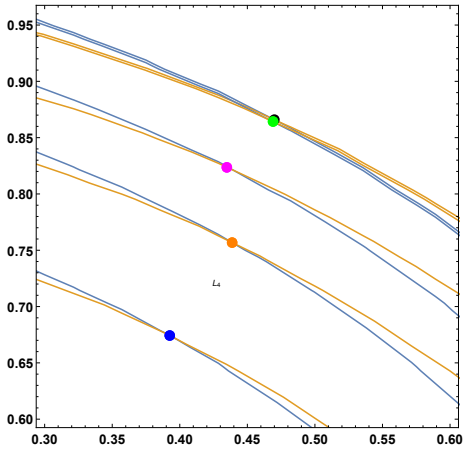

(b) Zoomed part of figure (1(a)) near L_4

Figure 1: Locations of equilibrium points in $\xi - \eta$–plane at $\mu = 0.03$

3.2 Poincaré surfaces of section

The aim of plotting the Poincaré surfaces of section is to examine the chaotic or regular behaviour of the path of the infinitesimal oblate body. The graph between ξ and $\dot{\xi}$ must be drawn when $\eta = 0$, whenever the orbit intersects the plane at $\dot{\eta} \geq 0$. Here we have plotted the Poincaré surfaces of section by creating a phase space in case 5 and given in Figures 5(a) and 5(b) in $\xi - \dot{\xi}$ and

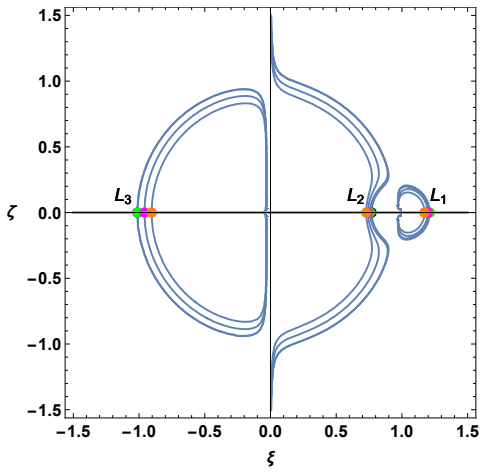

(a) Represents the first four cases 1 (black), 2 (green), 3 (magenta), 4 (orange)

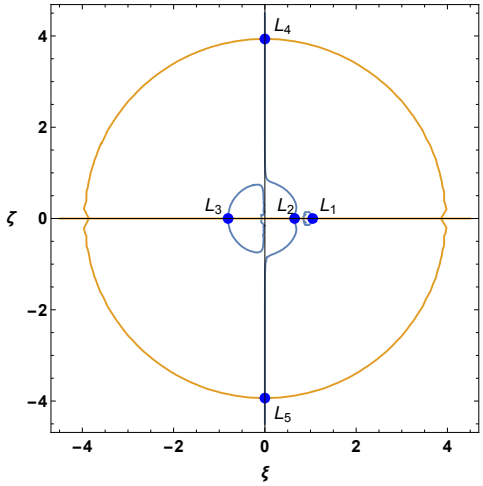

(b) Variation of mass case 5 (blue) i.e. $\alpha_1 = 0.2$ and $\alpha_2 = 0.4$

Figure 2: Locations of equilibrium points in $\xi - \zeta$–plane at $\mu = 0.03$

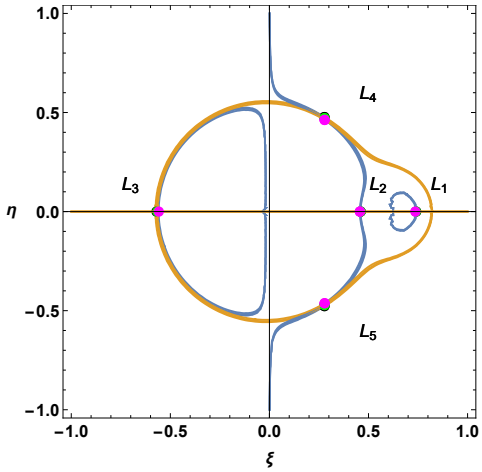

(a) Variation of mass parameter α_1 in $\xi - \eta$–plane

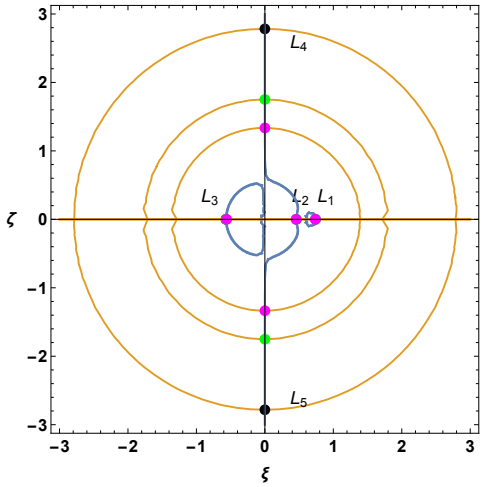

(b) Variation of mass parameter α_1 in $\xi - \zeta$–plane

Figure 3: Locations of equilibrium points at $\alpha_2 = 0.4, \alpha_1 = 0.2$ (black), 0.4 (green), 0.6 (magenta)

$\eta - \dot{\eta}$-planes respectively. We observed from these two figures that as the value of α_2 increases, the surfaces of section expanded and these appear as butterfly on the phase plane. In this way there are no chaos found in this study.

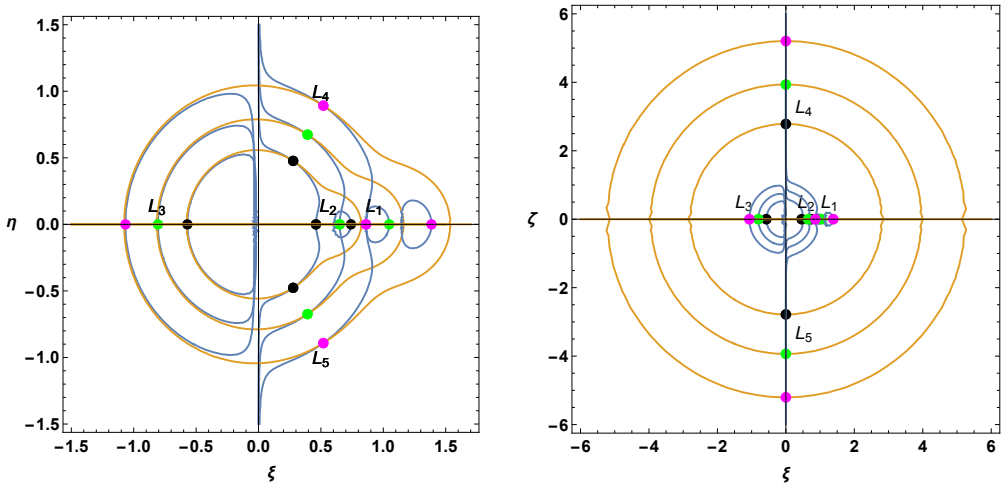

(a) Variation of mass parameter α_2 in $\xi - \eta$–plane

(b) Variation of mass parameter α_2 in $\xi - \zeta$–plane

Figure 4: Locations of equilibrium points at $\alpha_1 = 0.2, \alpha_2 = 0.4$ (black), 0.8 (green), 1.4 (magenta)

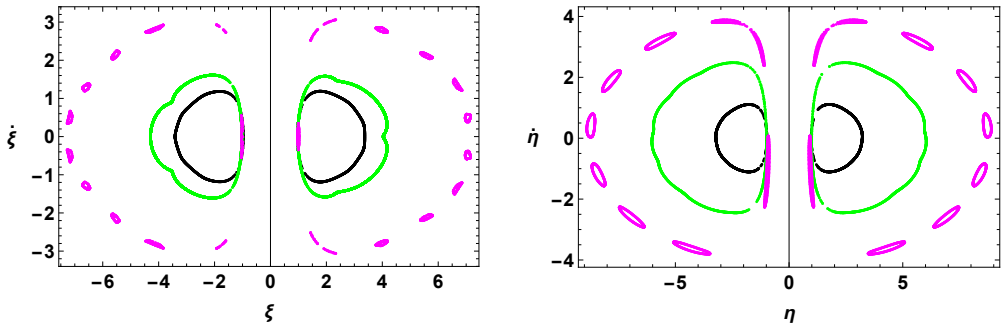

(a) Variation of mass parameter α_2 in $\xi - \dot{\xi}$–plane

(b) Variation of mass parameter α_2 in $\eta - \dot{\eta}$–plane

Figure 5: Poincaré surfaces of section at $\alpha_1 = 0.2, \alpha_2 = 0.4$ (black), 0.8 (green), 1.4 (magenta)

3.3 Regions of possible motion

To illustrate the regions of possible or forbidden motion, we follow the procedure and terminology used by [15]. To determine the each value of Jacobian constant corresponding to the each equilibrium point we use Eq. (7) and plotted gray shaded regions as the forbidden regions which are given in Figure (6). These figures reveal very important dynamical properties of the motion of the infinitesimal variable mass oblate body. Figure (6(a)) represents the region cor-

responding to the equilibrium point L_1 and shows that infinitesimal body can move near primaries except the gray color shaded region i. e. it can not move near $L_{2,3,4,5}$. It can move only near L_1 which is a gateway for the circular region. Figure (6(b)) represents the region corresponding to the equilibrium point L_2 and shows that the small particle can move freely except near the equilibrium points $L_{3,4,5}$. Figure (6(c)) represents the region corresponding to the equilibrium point L_3 and shows that the small particle can move near the three equilibrium points L_1, L_2 and L_3 where as it can not move in gray shaded regions i.e. near the equilibrium points $L_{4,5}$. Figure (6(d)) represents the region corresponding to the equilibrium points $L_{4,5}$ and shows that the small particle can move freely and there is no forbidden region. Blue points are indicating the locations of the equilibrium points.

3.4 Basins of attraction

One of the most important qualitative behaviour of the dynamical systems is the basins of attracting domain. To study this we use very simple and well known Newton-Raphson iterative method. Using this iterative method, we have illustrated the attracting domain in $\xi - \eta$-plane for different values of variation parameter (α_2). The algorithm of this problem is given as:

$$\xi_{n+1} = \xi_n - \left(\frac{\Omega_\xi \Omega_{\eta\eta} - \Omega_\eta \Omega_{\xi\eta}}{\Omega_{\xi\xi}\Omega_{\eta\eta} - \Omega_{\xi\eta}\Omega_{\eta\xi}} \right)_{(\xi_n, \eta_n)}, \tag{11}$$

$$\eta_{n+1} = \eta_n - \left(\frac{\Omega_\eta \Omega_{\xi\xi} - \Omega_\xi \Omega_{\eta\xi}}{\Omega_{\xi\xi}\Omega_{\eta\eta} - \Omega_{\xi\eta}\Omega_{\eta\xi}} \right)_{(\xi_n, \eta_n)}, \tag{12}$$

where ξ_n, η_n are the values of ξ and η coordinates of the n^{th} step of iterative process. The point (ξ, η) will be a member of the attracting domain, if the initial point converges rapidly to one of the equilibrium points. This process stops when the successive approximation converges to an equilibrium point. We also declare that the basins of attracting domain is not related with the classical basins of attracting domain in dissipative system. We used a color code for the classification of different equilibrium points on the $\xi - \eta$-plane.

We have performed the basins of attracting domain for three different values of variation parameter α_2 (0.4, 0.8 and 1.4 corresponds to the Figures 7, 8 and 9 respectively) in $\xi - \eta$-plane for the variable mass case 5. Figures 7(b), 8(b) and 9(b) are the zoomed parts of the Figures 7(a), 8(a) and 9(a) respectively. In all three figures, we observed that there are five attracting points $L_{1,2,3,4,5}$. From the Figure (7(b)), we found that $L_{1,2,3}$ corresponds to the light blue color region, L_4 corresponds to the blue color region and L_5 corresponds to the green color region, all these regions extended to infinity. From the Figure (8(b)), we found that $L_{1,2,3}$ corresponds to the green color region, L_4 corresponds to the cyan color region while L_5 corresponds to the red color region, all these regions extended to infinity. Further from the Figure (9(b)), we found that

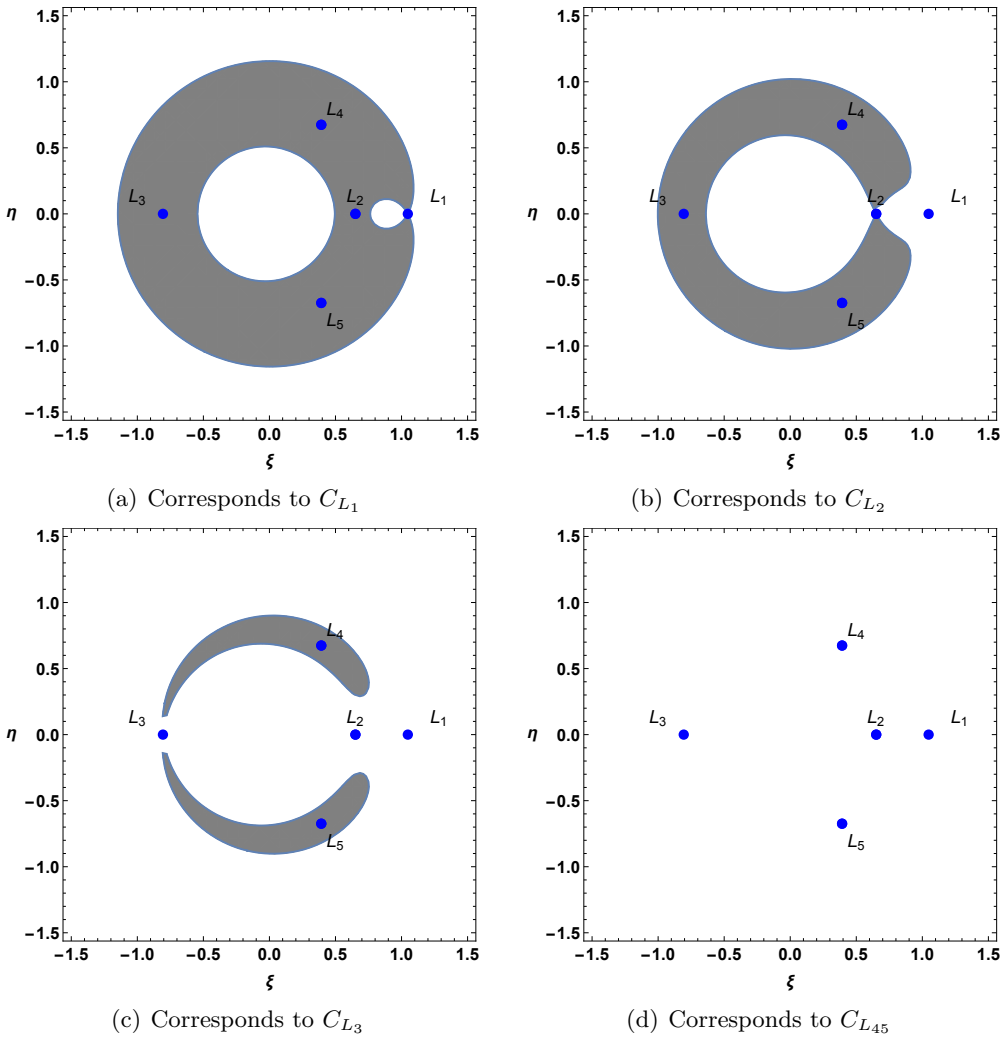

(a) Corresponds to C_{L_1}

(b) Corresponds to C_{L_2}

(c) Corresponds to C_{L_3}

(d) Corresponds to $C_{L_{45}}$

Figure 6: Regions of motion in $\xi - \eta$–plane corresponding to the variable mass case 5

$L_{1,2,3}$ corresponds to the green color region, L_4 corresponds to the purple color region and L_5 corresponds to the red color region, all these regions extended to infinity. In all the figures black dots are denoting the locations of the attracting points.

4. Stability of equilibrium points

In this section we examine the stability of equilibrium points of the infinitesimal variable mass oblate body in the neighbourhood of $(\xi_0 + \xi_1, \eta_0 + \eta_1, \zeta_0 + \zeta_1)$ under the effect of the oblate radiating primaries and the perturbing factors of

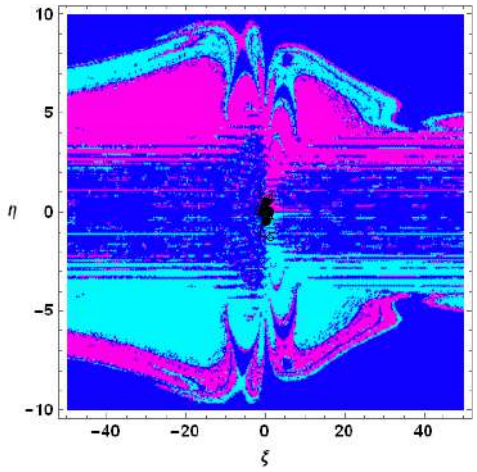

(a) Corresponds to $\alpha_1 = 0.2, \alpha_2 = 0.4$

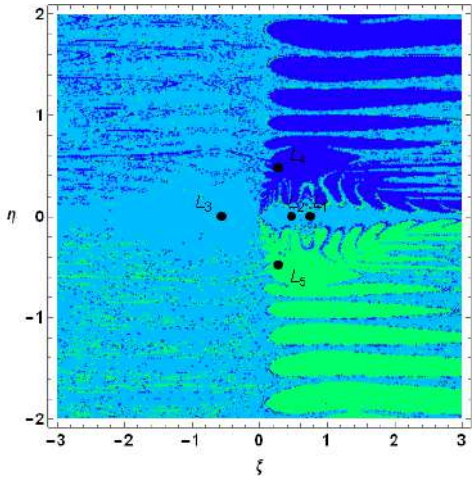

(b) Zoomed part of figure 7(a) near center of mass

Figure 7: Basins of Attracting domain corresponding to variable mass case 5 in $\xi - \eta$–plane

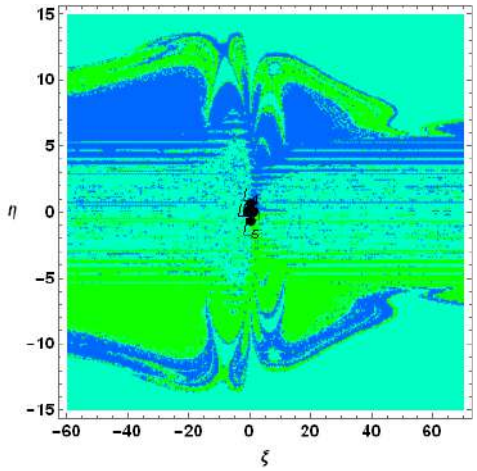

(a) Corresponds to $\alpha_1 = 0.2, \alpha_2 = 0.8$

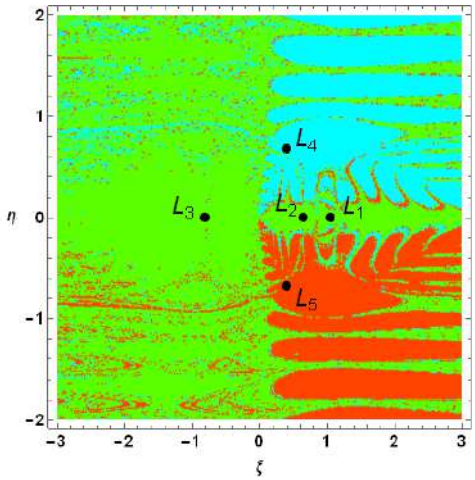

(b) Zoomed part of figure 8(a) near center of mass

Figure 8: Basins of Attracting domain corresponding to variable mass case 5 in $\xi - \eta$–plane

Coriolis and centrifugal forces. Where (ξ_1, η_1, ζ_1) are small displacements from the equilibrium points (ξ_0, η_0, ζ_0).

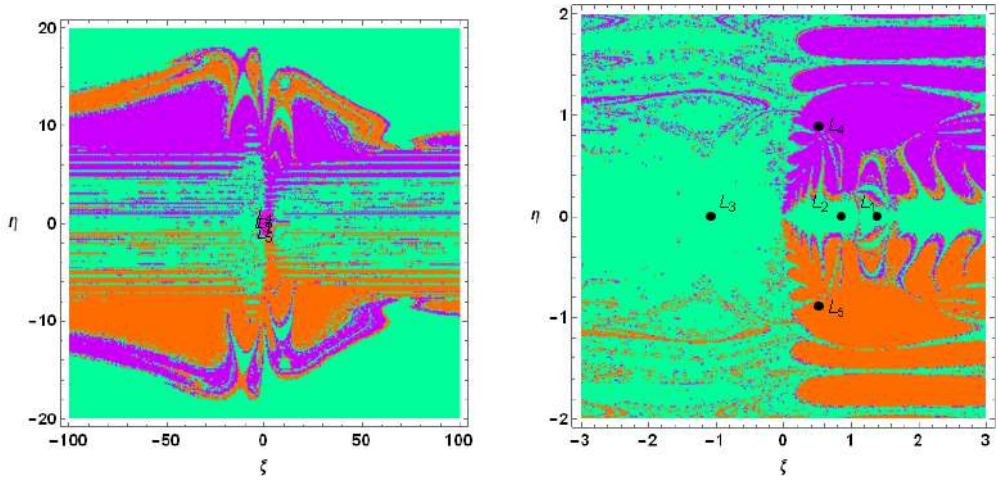

(a) Corresponds to $\alpha_1 = 0.2, \alpha_2 = 1.4$

(b) Zoomed part of figure 9(a) near center of mass

Figure 9: Basins of Attracting domain corresponding to variable mass case 5 in $\xi - \eta$–plane

The system (4) can be rewritten in the phase space as:

$$
\begin{aligned}
\dot{\xi_1} &= \xi_2, \\
\dot{\eta_1} &= \eta_2, \\
\dot{\zeta_1} &= \zeta_2, \\
\dot{\xi_2} &= 2n\phi\eta_2 + (\Omega_{\xi\xi})^0\xi_1 + (\Omega_{\xi\eta})^0\eta_1 + (\Omega_{\xi\zeta})^0\zeta_1, \\
\dot{\eta_2} &= -2n\phi\xi_2 + (\Omega_{\eta\xi})^0\xi_1 + (\Omega_{\eta\eta})^0\eta_1 + (\Omega_{\eta\zeta})^0\zeta_1, \\
\dot{\zeta_2} &= (\Omega_{\zeta\xi})^0\xi_1 + (\Omega_{\zeta\eta})^0\eta_1 + (\Omega_{\zeta\zeta})^0\zeta_1,
\end{aligned} \tag{13}
$$

where the superscript 0 indicates the value of the second derivative of potential function at the corresponding equilibrium point (ξ_0, η_0, ζ_0).

When $\alpha_1 = 0$, then the above system (13) will reduce to the constant mass, while when $\alpha_1 \neq 0$, then we can not examine the stability by ordinary method because the distances of the equilibrium point to the primaries vary with time. Therefore we will use Meshcherskii-space-time inverse transformations which are as follows:

$$
\begin{aligned}
\xi_3 =& \alpha_2^{-1/2}\xi_1, \eta_3 = \alpha_2^{-1/2}\eta_1, \zeta_3 = \alpha_2^{-1/2}\zeta_1, \\
\xi_4 =& \alpha_2^{-1/2}\xi_2, \eta_4 = \alpha_2^{-1/2}\eta_2, \zeta_4 = \alpha_2^{-1/2}\zeta_2.
\end{aligned} \tag{14}
$$

Using the transformations given in Eq. (14), the system (13) can be written as follows:

$$\dot{\chi} = A\ \chi, \tag{15}$$

where

$$\dot{\chi} = \begin{pmatrix} \dot{\xi}_3 \\ \dot{\eta}_3 \\ \dot{\zeta}_3 \\ \dot{\xi}_4 \\ \dot{\eta}_4 \\ \dot{\zeta}_4 \end{pmatrix}, \chi = \begin{pmatrix} \xi_3 \\ \eta_3 \\ \zeta_3 \\ \xi_4 \\ \eta_4 \\ \zeta_4 \end{pmatrix} \tag{16}$$

and

$$A = \begin{pmatrix} \frac{1}{2}\alpha_1 & 0 & 0 & 1 & 0 & 0 \\ 0 & \frac{1}{2}\alpha_1 & 0 & 0 & 1 & 0 \\ 0 & 0 & \frac{1}{2}\alpha_1 & 0 & 0 & 1 \\ (\Omega_{\xi\xi})^0 & (\Omega_{\xi\eta})^0 & (\Omega_{\xi\zeta})^0 & \frac{1}{2}\alpha_1 & 2n\phi & 0 \\ (\Omega_{\eta\xi})^0 & (\Omega_{\eta\eta})^0 & (\Omega_{\eta\zeta})^0 & -2n\phi & \frac{1}{2}\alpha_1 & 0 \\ (\Omega_{\zeta\xi})^0 & (\Omega_{\zeta\eta})^0 & (\Omega_{\zeta\zeta})^0 & 0 & 0 & \frac{1}{2}\alpha_1 \end{pmatrix} \tag{17}$$

The characteristic equation for the matrix A is

$$\lambda^6 + \beta_5\ \lambda^5 + \beta_4\ \lambda^4 + \beta_3\ \lambda^3 + \beta_2\ \lambda^2 + \beta_1\ \lambda + \beta_0 = 0, \tag{18}$$

where

$$\begin{aligned}
\beta_5 &= -3\alpha_1, \\
\beta_4 &= 4n^2\phi^2 - (\Omega_{\xi\xi})^0 - (\Omega_{\eta\eta})^0 - (\Omega_{\zeta\zeta})^0 + \frac{15}{4}\alpha_1^2, \\
\beta_3 &= 2\alpha_1((\Omega_{\xi\xi})^0 + (\Omega_{\eta\eta})^0 + (\Omega_{\zeta\zeta})^0 - 8n^2\phi^2 - \frac{5}{4}\alpha_1^2), \\
\beta_2 &= \frac{1}{64}\alpha_1^2(384n^2\phi^2 + 60\alpha_1^2 - 96((\Omega_{\xi\xi})^0 + (\Omega_{\eta\eta})^0 + (\Omega_{\zeta\zeta})^0)) \\
&\quad - (4n^2\phi^2(\Omega_{\zeta\zeta})^0 + ((\Omega_{\xi\eta})^0)^2 + ((\Omega_{\xi\zeta})^0)^2 - (\Omega_{\xi\xi})^0(\Omega_{\eta\eta})^0 \\
&\quad + ((\Omega_{\eta\zeta})^0)^2 - (\Omega_{\xi\xi})^0(\Omega_{\zeta\zeta})^0 - (\Omega_{\eta\eta})^0(\Omega_{\zeta\zeta})^0), \\
\beta_1 &= \frac{1}{64}\alpha_1^3(32((\Omega_{\xi\xi})^0 + (\Omega_{\eta\eta})^0 + (\Omega_{\zeta\zeta})^0 - 4n^2\phi^2) - 12\alpha_1^2) \\
&\quad + \alpha_1(((\Omega_{\xi\eta})^0)^2 + ((\Omega_{\xi\zeta})^0)^2 - (\Omega_{\xi\xi})^0(\Omega_{\eta\eta})^0
\end{aligned} \tag{19}$$

$$
\begin{aligned}
&+((\Omega_{\eta\zeta})^0)^2-(\Omega_{\xi\xi})^0(\Omega_{\zeta\zeta})^0-(\Omega_{\eta\eta})^0(\Omega_{\zeta\zeta})^0+4n^2\phi^2(\Omega_{\zeta\zeta})^0,\\
\beta_0 &= \frac{\alpha_1^4}{64}(-4((\Omega_{\xi\xi})^0+(\Omega_{\eta\eta})^0+(\Omega_{\zeta\zeta})^0-4n^2\phi^2)+\alpha^2)\\
&+\frac{\alpha_1^2}{4}(((\Omega_{\xi\zeta})^0)^2-((\Omega_{\xi\eta})^0)^2+(\Omega_{\xi\xi})^0(\Omega_{\eta\eta})^0\\
&-((\Omega_{\eta\zeta})^0)^2+(\Omega_{\xi\xi})^0(\Omega_{\zeta\zeta})^0+(\Omega_{\eta\eta})^0(\Omega_{\zeta\zeta})^0-n^2\phi^2(\Omega_{\zeta\zeta})^0)\\
&+((\Omega_{\xi\zeta})^0)^2(\Omega_{\eta\eta})^0-2(\Omega_{\xi\eta})^0(\Omega_{\xi\zeta})^0(\Omega_{\eta\zeta})^0+(\Omega_{\xi\xi})^0((\Omega_{\eta\zeta})^0)^2\\
&+((\Omega_{\xi\eta})^0)^2(\Omega_{\zeta\zeta})^0-(\Omega_{\xi\xi})^0(\Omega_{\eta\eta})^0(\Omega_{\zeta\zeta})^0.
\end{aligned}
$$

We solved equation (18) numerically for different values of parameters used and evaluated the characteristic roots for each equilibrium points which are given in table 1. From this table we observed that all the equilibrium points are unstable because at-least one characteristic root is either positive real number or positive real part of the complex characteristic root. While in the classical case collinear equilibrium points are always unstable and triangular equilibrium points are stable [28]. Therefore, the variation parameters changes the stability of equilibrium points to instability.

Table 1: The nature of equilibrium points in $\xi-\eta$-plane at $\alpha_1=0.2$, $\alpha_2=0.4$, $\mu=0.03$, $q_1=0.85$,$q_2=0.95$,$\sigma=0.001$, $\sigma_1=0.003$, $\sigma_2=0.005$, $\epsilon_1=0.2$, $\epsilon_2=0.2$.

EquilibriumPoint		*Roots*	*Nature*
$\xi-Co.$	$\eta-Co.$		
0.7408249862	0.0000000000	$0.0999999999\pm 2.2972215331i$ $0.0999999999\pm 2.1773781596i$ -2.7663246283 2.9663246283	*Unstable*
0.4602562445	0.0000000000	$0.1000000002\pm 2.0542780618i$ $0.1000000009\pm 2.2072142439i$ -2.4264415713 2.6264415713	*Unstable*
-0.5699707318	0.0000000000	$0.0999999992\pm 1.1187298304i$ $0.1000000007\pm 1.4706767196i$ -0.1544263628 0.3544263628	*Unstable*
0.2775860568	± 0.4767832700	$0.0999999995\pm 0.4141521317i$ $0.1000000006\pm 1.1019981851i$ $0.1000000009\pm 1.4017456238i$	*Unstable*

5. Conclusion

The effects of parameters used are studied in the perturbed circular restricted three-body problem where infinitesimal oblate body varies its mass according to Jean's law and both the primaries are having radiation as well as oblateness effects. And the system is also affected by the perturbing factor in Coriolis and centrifugal forces. The equations of motion are evaluated by using Jeans law and Meshcherskii-space time transformations, our determined system differs by the variation parameters (α_1 and α_2) from the classical case 1. We have numerically and graphically shown the equilibrium points, Poincaré surfaces of section, regions of possible and forbidden motion and also basins of attracting domain with the different values of parameters used. Here at most five equilibrium points are obtained, out of which three are collinear (L_1, L_2 and L_3) and other two are non-collinear (L_4 and L_5)(Figures 1, 2, 3 and 4). As we introduce one by one cases (from case 1 to case 5) in the system (4) for equilibrium points, Figures 1 and 2 show that all the equilibrium points are moving towards origin. Figure 3 represents the locations of equilibrium points with the change in variation parameter α_1, from here we found that all the equilibrium points are moving toward origin in $\xi - \zeta$-plane while in $\xi - \eta$-plane, it has little effect. Figure 4 performs the change in the variation parameter α_2, and we observed that equilibrium points are moving away from the origin in both $\xi - \eta$ and $\xi - \zeta$-planes. To study the dynamical behaviour of the infinitesimal oblate body, we have plotted the Poincaré surfaces of section and found regular curves with many islands which appear like a butterfly (Figure 5). Next we have determined the value of Jacobi-constant corresponding to each equilibrium points by using the method given by [15] and illustrated the prohibited and allowed regions for the infinitesimal oblate body. Here gray shaded regions are the forbidden regions (Figure 6) and in the rest part infinitesimal body can move freely. Further more we have drawn the basins of attracting domain for three different values of α_2 and given in Figures (7, 8 and 9). From these figures we obtained different color regions which are showing the different attracting domain. Finally we performed the stability of equilibrium points numerically. This numerical study is given in the table 1. From this table we observed that at least one of the roots have either positive real part of the complex roots or only positive real root. Which confirm that all the equilibrium points are unstable. This result is different from the result obtained in classical case [28], where we found that three equilibrium points are unstable while two are stable. Therefore these variation parameters have great impact on the dynamical behaviour of the motion of the infinitesimal variable mass oblate body.

References

[1] A. AbdulRaheem, J. Singh, *Combined effects of perturbations, radiation, and oblateness on the stability of equilibrium points in the restricted three-*

body problem, Astron. J., 131 (2006), 1880–1885.

[2] E. I. Abouelmagd, A. A. Ansari, M. S. Ullah, J. L. G. Guirao, *A planar five-body problem in a framework of heterogeneous and mass variation effects*, The Astronomical Journal, 160 (2020), 216.

[3] E. I. Abouelmagd, H. M. Asiri, M. A. Sharaf, *The effect of oblateness in the perturbed restricted three-body problem*, Meccanica, 48 (2013), 2479–2490.

[4] E. I. Abouelmagd, S. M. El-Shaboury, *Periodic orbits under combined effects of oblateness and radiation in the restricted problem of three bodies*, Astrophys. Space Sci., 341 (2012), 331–341.

[5] E. I. Abouelmagd, A. A. Ansari, *The motion properties of the infinitesimal body in the framework of bicircular Sun-perturbed Earth-Moon system*, New Astronomy, 73 (2019), 101282.

[6] E. I. Abouelmagd, A. Mostafa, *Out of plane equilibrium points locations and the forbidden movement regions in the restricted three-body problem with variable mass*, Astrophys. Space Sci., 357 (2015), 58.

[7] A. A. Ansari, K. R. Meena, S. N. Prasad, *Perturbed six-body configuration with variable mass*, Romanian Astronomical Journal, 30 (2020), 135-152.

[8] A. A. Ansari, E. I. Abouelmagd, *Gravitational potential formulae between two bodies with finite dimensions*, Astronomical Notes, (2020).

[9] A. A. Ansari, et al., *The motion properties of the variable mass planetoid in the elliptical Sitnikov problem*, Gedrag & Organisatie Review, 33 (2020), 398-405.

[10] A. A. Ansari, S. N. Prasad, M. Alam, *Variable mass of a test particle in Copenhagen problem with Manev-type potential*, Research and review journal for Physics, 9 (2020), 17-27.

[11] A. A. Ansari, *Kind of Robe's restricted problem with heterogeneous irregular primary of N-layers when outer most layer has viscous fluid*, New Astronomy, 83 (2020).

[12] A. A. Ansari, et al., *Perturbed Robe's CR3BP with Viscous Force*, Astrophys. Space Sci., 364 (2019), 95.

[13] A. A. Ansari, et al., *Effect of charge in the circular restricted three-body problem with variable masses*, Journal of Taibah University for Science, 13 (2019), 670-677.

[14] A. A. Ansari, et al., *Behavior of an infinitesimal-variable-mass body in CR3BP; the primaries are finite straight segments*, Punjab University Journal of Mathematics, 51 (2019), 107-120.

[15] A. A. Ansari, Z. A. Alhussain, S. N. Prasad, *Circular restricted three-body problem when both the primaries are heterogeneous spheroid of three layers and infinitesimal body varies its mass*, Journal of Astrophysics and Astronomy, 39 (2018), 57.

[16] A. A. Ansari, *Effect of Albedo on the motion of the infinitesimal body in circular restricted three-body problem with variable masses*, Italian Journal of Pure and Applied Mathematics, 38 (2017), 581-600.

[17] K. B. Bhatnagar, P. P. Hallan, *Effect of perturbations in Coriolis and centrifugal forces on the stability of libration points in the restricted problem*, Celestial Mechanics, 18 (1978), 105–112.

[18] C. N. Douskos, *Collinear equilibrium points of Hill's problem with radiation pressure and oblateness and their fractal basins of attraction*, Astrophys. Space Sci., 326 (2010), 263–271.

[19] J. H. Jeans, *Astronomy and cosmogony*, Cambridge University Press, Cambridge, 1928.

[20] R. Kumari, B. S. Kushvah, *Equilibrium points and zero velocity surfaces in the restricted four-body problem with solar wind drag*, Astrophys. Space Sci., 344 (2013), 347–359.

[21] L. G. Lukyanov, *On the restricted circular conservative three-body problem with variable masses*, Astronomy Letters, 35 (2009), 349-359.

[22] I. V. Meshcherskii, *Works on the mechanics of bodies of variable mass*, GITTL, Moscow, 1949.

[23] A. S. Beevi, R. K. Sharma, *Oblateness effect of Saturn on periodic orbits in the Saturn-Titan restricted three-body problem*, Astrophys. Space Sci., 340 (2012), 245–261.

[24] K. Shalini, A. A. Ansari, F. Ahmad, *Existence and stability of L_4 of the R3BP when the smaller primary is a heterogeneous triaxial rigid body with N layers*, J. Appl. Environ. Biol. Sci., 6 (2016), 249-257.

[25] R. K. Sharma, P. V. SubbaRao, *Stationary solutions and their characteristic exponents in the restricted three-body problem when the more massive primary is an oblate spheroid*, Celestial Mechanics, 13 (1976), 137-149.

[26] J. Singh, B. Ishwar, *Effect of perturbations on the stability of triangular points in the restricted problem of three bodies with variable mass*, Celestial Mechanics, 35 (1985), 201-207.

[27] J. Singh, J. J. Taura, *Motion in the generalized restricted three-body problem*, Astrophys. Space Sci., 343 (2013), 95–106.

[28] V. Szebehely, *Theory of orbits*, Academic Press, New York, 1967.

[29] M. J. Zhang, C. Y. Zhao, Y. Q. Xiong, *On the triangular libration points in photo-gravitational restricted three-body problem with variable mass*, Astrophys. Space Sci., 337 (2012), 107-113.

[30] E. E. Zotos, W. Chen, E. I. Abouelmagd, H. Han, *Basins of convergence of equilibrium points in the restricted three-body problem with modified gravitational potential*, Chaos, Solitons and Fractals, 134 (2020), 109704.

Accepted: October 21, 2020